Molecular-orbital decomposition of the ionization continuum for a diatomic molecule by angle- and energy-resolved photoelectron spectroscopy. II. Ionization continuum of NO

Hongkun Park and Richard N. Zare
Department of Chemistry, Stanford University, Stanford, California 94305

(Received 19 September 1995; accepted 12 December 1995)

The quantum-state-specific photoelectron angular distributions (PADs) from the NO $A\ ^2\Sigma^+(\nu=0,\ N)$ and $D\ ^2\Sigma^+(\nu=0,\ N)$ states are analyzed based on the theoretical formalism presented in the preceding companion article. The dynamical parameters in this analysis can be divided into two distinct types, one that directly pertains to the dynamics in the ionization continuum of NO that yields the $NO^+\ X\ ^1\Sigma^+(\nu^+=0,\ N^+)$ ion and the other that depends both on the ionizing state and on the ionization continuum. The continuum parameters obtained in this study determine various molecule-frame scattering matrices that describe the short-range collision dynamics between the photoelectron and the $NO^+\ X\ ^1\Sigma^+(\nu^+=0,\ N^+)$ core and agree very well with the corresponding quantum-defect quantities determined for high-lying Rydberg states converging to the $NO^+\ X\ ^1\Sigma^+(\nu^+=0,\ N^+)$ ion. Specifically, it is found that $s\sigma$- and $d\sigma$-partial waves mix almost completely because of the anisotropic interactions between the photoelectron and the other electrons in the ion core whereas the orbital angular momentum of the other partial waves are relatively unperturbed by scattering with the ion core. The dynamical parameters determined in the analysis also constitute complete descriptions of the photoionization events of the NO $A\ ^2\Sigma^+(\nu=0,\ N)$ and $D\ ^2\Sigma^+(\nu=0,\ N)$ states and provide detailed quantitative information about the Cooper minimum in the $3p\sigma\rightarrow d\sigma$ ionization channel that appears in the photoionization of the NO $D\ ^2\Sigma^+(\nu=0)$ state. The present study represents the first direct experimental determination of the scattering dynamics between the photoelectron and the ion core in a molecular system. © *1996 American Institute of Physics.* [S0021-9606(96)00711-1]

I. INTRODUCTION

The close connection between the dynamics in the ionization continuum reached in a photoionization process and that of the Rydberg states has long been recognized in atomic physics.[1] Despite their different asymptotic behaviors, electrons in the ionization continuum and in Rydberg states share common physics at the short electron–ion-core distance that can be described as the scattering of the photoelectron and the ion. Hence, photoelectron spectroscopy and spectroscopy of Rydberg states provide complementary information on the short-range scattering dynamics between the electron and the ion. The realization of this commonality between the dynamics in the ionization continuum and that of the Rydberg states has played an essential role in providing a unified description of diverse experimental data, such as the quantum defects of Rydberg series, perturbations between Rydberg levels, and photoelectron angular distributions (PADs) from direct and resonant photoionization events.[2–7]

In molecular systems, the same commonality between the dynamics in the ionization continuum and that of the Rydberg states exists despite the complexities introduced by reduced symmetry, the structure of the ion core, and the presence of nuclear degrees of freedom.[8,9] However, direct experimental investigations of the short-range scattering dynamics between the electron and the molecular ion using photoelectron spectroscopy are lacking, and our current knowledge on this subject has been derived almost exclusively from *ab initio* investigations[10–12] and analyses of Rydberg levels based on the multichannel quantum defect theory (MQDT).[9,13–16]

The recent advent of various photoelectron-spectroscopic techniques that accomplish the resolution of individual quantum levels of ion has enabled detailed investigation of the dynamics of molecular photoionization.[17–21] By analyzing quantum-state-specific PADs from optically aligned molecules in a specific quantum level that is accessed by resonance-enhanced multiphoton ionization (REMPI), it has been shown that even the complete information that describes the molecular photoionization process can be obtained experimentally.[20,22–26] A natural extension to these studies is then to employ these photoelectron-spectroscopic techniques to investigate the short-range scattering dynamics between the photoelectron and the ion to complement the information obtained by bound-state Rydberg spectroscopy.

In the companion article (abbreviated hereafter as PZ1[27]), we developed a theoretical formalism based on the molecular-orbital decomposition of the ionization continuum that treats explicitly the short-range scattering between the photoelectron and the molecular ion within the independent electron approximation. The most notable feature of the theoretical formalism is that the dynamical parameters in it can be classified into two distinct types, one that pertains only to the ionization continuum and the other that depends both on the ionizing state and on the ionization continuum. Through this disentanglement of the ionization-continuum dynamics from the photoionization dynamics, the formalism exploits maximally the commonality between different photoionization processes and allows for the direct extraction of dynamical information that pertains to the ionization continuum by analyzing the quantum-state-specific PADs from multiple electronic states.

In this article, the theoretical formalism in PZ1 is applied to analyze the quantum-state-specific PADs of the NO $A\,^2\Sigma^+(\nu=0,\,N)$ and $D\,^2\Sigma^+(\nu=0,\,N)$ states and to obtain dynamical parameters that describe both the dynamics in the ionization continuum of NO associated with the formation of the NO^+ $X\,^2\Sigma^+(\nu^+=0,\,N^+)$ ion *and* the photoionization dynamics of the NO A and D states. Through simultaneous analysis of the quantum-state-specific PADs from the NO A and D states, the dynamical parameters that pertain directly to the ionization continuum are determined in this study. These continuum parameters, which characterize the properties of continuum molecular orbitals in the ionization continuum of NO, determine various molecule-frame scattering matrices up to a phase factor and provide detailed quantitative insight into the collision dynamics between the photoelectron and the NO^+ $X\,^2\Sigma^+(\nu^+=0,\,N^+)$ ion. The continuum parameters determined in this study can also be compared directly with the MQDT parameters that are obtained from analysis of the high-lying Rydberg states converging to the NO^+ $X\,^2\Sigma^+(\nu^+=0,\,N^+)$ ion. The comparison shows good overall agreement between the parameters determined in our analysis and the MQDT parameters, thus illustrating that the quantum-state-specific PADs can provide dynamical information complementary to that obtained from spectroscopy of Rydberg states.

In addition to providing dynamical information about the ionization continuum, the dynamical parameters obtained from the simultaneous fit provide complete descriptions of the photoionization dynamics of the NO $A\,^2\Sigma^+(\nu=0)$ and $D\,^2\Sigma^+(\nu=0)$ states.[23–25,28,29] Hence, the dynamical parameters determined in this study enable us to predict experimentally unobserved quantities such as the three-dimensional PADs and the angular-momentum polarizations of the ions produced from the photoionization process.[22,24,25] They also provide conclusive experimental evidence for the existence of a Cooper minimum in the $3p\sigma\rightarrow d\sigma$ ionization channel in the photoionization of the NO $D\,^2\Sigma^+(\nu=0)$ state.

A complete description of a molecular photoionization event has already been accomplished for the photoionization of the NO $A\,^2\Sigma^+(\nu=0)$ state by analyzing quantum-state-specific PADs using the theoretical formalism based on the partial-wave decomposition of the ionization continuum.[23–25] It is worthwhile to note, however, that in the present study, a complete description of the NO D state has been achieved without measurement of the circular dichroism in PADs (CDAD).[23,24,30–32] As shown in our previous study, the measurement of CDAD is necessary to determine the signs of phases of dipole-moment matrix elements within the context of the partial-wave theoretical formalism.[23–25] In the present analysis, which is based on the molecular-orbital decomposition of the ionization continuum, the CDAD measurement for photoionization of the NO A state alone provides enough experimental constraints for us to determine completely dynamical parameters that describe the photoionization dynamics of the NO A *and* D states. This determination is a clear demonstration of the advantage of the molecular-orbital formalism presented in PZ1 that exploits the commonality between distinct photoionization processes.

II. ANALYSIS OF EXPERIMENTAL PADS: EXTRACTION OF DYNAMICAL PARAMETERS

The quantum-state-specific PADs from the NO $A\,^2\Sigma^+(\nu=0,\,N)$ and $D\,^2\Sigma^+(\nu=0,\,N)$ states reported previously[20,24,26] are analyzed here based on the theoretical formalism presented in PZ1. Three data sets are included in the analysis: The first set of data consists of quantum-state-specific PADs from photoionization of the NO $A\,^2\Sigma^+(\nu=0,\,N=25)$ level via the $A\,^2\Sigma^+-X\,^2\Pi(0-0)P_{21}+Q_1(25.5)$ excitation employing linearly polarized excitation and ionization light beams at 225.4 and 312 nm, respectively.[20] The second set consists of PADs from photoionization of the NO $A\,^2\Sigma^+(\nu=0,\,N=22)$ level via the $A\,^2\Sigma^+-X\,^2\Pi(0-0)P_{21}+Q_1(22.5)$ excitation employing linearly polarized excitation and circularly polarized ionization light beams at 225.6 and 313.5 nm, respectively.[24] The third set contains PADs from photoionization of the NO $D\,^2\Sigma^+(\nu=0,\,N=18)$ level via the $D\,^2\Sigma^+-X\,^2\Pi(0-0)Q_{21}+R_1(17.5)$ excitation employing linearly polarized excitation and ionization light beams at 187.2 and 428 nm, respectively.[26]

Figure 1 shows polar plots of experimental PADs for five ion rotational levels that result from photoionization of the NO $A\,^2\Sigma^+(\nu=0,\,N=25)$ level with linearly polarized excitation and ionization light beams. Each ionizing transition is labeled with $\Delta N=N^+-N$, which is the difference in the rotational quantum number of the ion and that of the ionizing state. The angle between the linear polarization vectors of the excitation and ionization laser beams is denoted as θ_T. Figure 2 shows polar plots of PADs observed in the photoionization of the NO $A\,^2\Sigma^+(\nu=0,\,N=22)$ level with linearly polarized excitation and circularly polarized ionization light beams. The difference in PADs that result from photoionization with left- and right-circularly polarized light beams constitutes the CDAD.[23,24,30–32] Finally, Fig. 3 shows polar plots of PADs observed from photoionization of the NO $D\,^2\Sigma^+(\nu=0,\,N=18)$ level when both the excitation and the ionization light beams are linearly polarized. In the PADs presented in Figs. 1–3, the error bar associated with each data point represents $\pm 2\sigma$ uncertainty. These quantum-state-specific PADs show a dramatic difference in nodal patterns depending on the electronic state being ionized, the value of ΔN, and the polarizations of the excitation and ionization light beams. Inspection of PADs also reveals that the angle-integrated cross sections and shapes of PADs for $\Delta N>0$ and $\Delta N<0$ transitions with the same $|\Delta N|$ are different for photoionization of the NO D state, whereas those of the corresponding PADs from the NO A state are approximately the same.[20,24,26]

In our formalism, the $(1+1')$ REMPI of NO is treated as

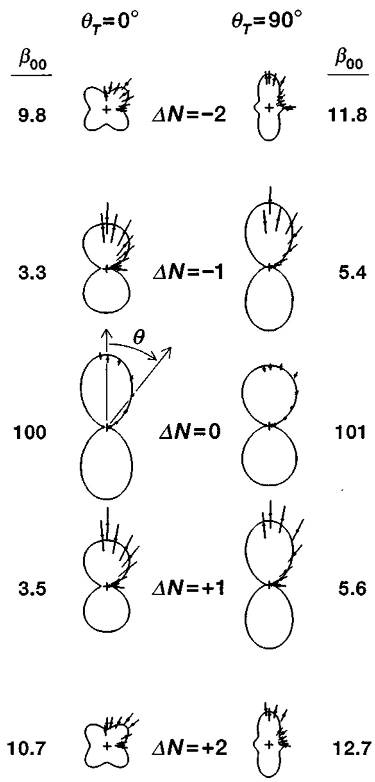

FIG. 1. Polar plots of experimental PADs for five ion rotational levels from photoionization of the NO $A\,^2\Sigma^+(v=0,\ N=25)$ level. Both the excitation- and the ionization-laser beams are linearly polarized. The plots are scaled to uniform size. The angle-integrated relative cross sections β_{00} are listed with the PADs. Note that the values of β_{00} for $\Delta N>0$ and $\Delta N<0$ transitions with the same $|\Delta N|$ are approximately the same. The error bars represent 2σ uncertainties. The solid lines are the predictions of the model based on the fit results listed in the second columns of Tables I through III.

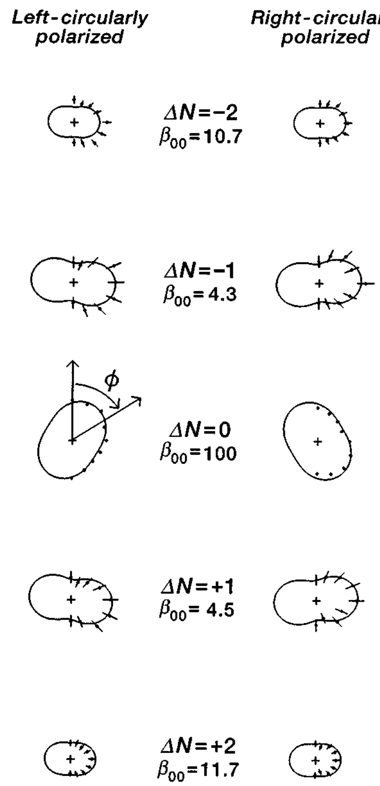

FIG. 2. Polar plots of experimental PADs for five ion rotational levels from photoionization of the NO $A\,^2\Sigma^+(v=0,\ N=22)$ level. The ionization-laser beam is circularly polarized, and the PADs are recorded by rotating the linear polarization vector of the excitation-light beam. The plots are scaled to uniform size. The angle-integrated relative cross sections β_{00} are listed with the PADs. The error bars represent 2σ uncertainties. The solid lines are the predictions of the model based on the fit results listed in the second columns of Tables I through III.

a two-step process consisting of the one-photon excitation step to the resonant intermediate state and the one-photon ionization step;[33] the one-photon excitation simply generates the aligned ionizing state, which is subsequently probed by the ionizing photon. Both the NO $A\,^2\Sigma^+(v=0)$ and $D\,^2\Sigma^+(v=0)$ states follow Hund's case (b) coupling, as evidenced by their small spin-rotation coupling constants.[34] Because the resonant excitation process in our experiment prepares a specific vibration-rotation level (v,N) in the ionizing state that follows Hund's case (b) coupling, the effect of the excitation step on PADs can be compactly represented in terms of the density matrix elements $\rho^N_{M_N M'_N}$ (or equivalently in terms of the spherical multipoles) that describe the distribution of the magnetic sublevels for the given (v,N) level.[24,27,35] The transitions employed to reach both the $A\,^2\Sigma^+(v=0,\ N)$ and $D\,^2\Sigma^+(v=0,\ N)$ levels are blended, and a mixture of two J levels with the same value of N are incoherently excited in the intermediate states.[20] It has been shown both experimentally[25] and theoretically,[36,37] however, that the electronic spin in the intermediate state does not affect the photoionization dynamics of the NO A and D states, which assures us that $\rho^N_{M_N M'_N}$ is sufficient to describe the effect of the excitation step on PADs. The expressions for $\rho^N_{M_N M'_N}$ can be found in Refs. 35 and 24, depending on whether the polarization of the ionization light beam is linear or circular.

Once the expressions for $\rho^N_{M_N M'_N}$ are obtained analytically for each experimental geometry, the observed quantum-state-specific PADs can be fit to Eqs. (42) and (43) in PZ1. The Levenberg–Marquadt modified nonlinear least-squares method was used in the fitting procedure, and the chi-square value served as the figure-of-merit function.[38] The parameters in the fit are eigenchannel parameters $\bar{U}^\lambda_{l\alpha_\lambda}$, $\bar{\tau}^\lambda_{\alpha_\lambda}$, and $M^\lambda_{\alpha_\lambda}$: $\bar{U}^\lambda_{l\alpha_\lambda}$ represents the vibrationally averaged value of the electronic transformation matrix element, $\bar{\tau}^\lambda_{\alpha_\lambda}$ represents the electronic eigenphase shift that is the scattering phase shift for the α_λth continuum molecular orbital, and $M^\lambda_{\alpha_\lambda}$ represents the vibrationally averaged electronic dipole-moment matrix element that connects a given ionizing electronic orbital to the α_λth continuum molecular orbital.[27] As emphasized in PZ1, these parameters specify not only the photoionization dynamics of the NO $A\,^2\Sigma^+(v=0)$ and $D\,^2\Sigma^+(v=0)$ states but also the dynamics in the ionization continuum of NO that yields the $NO^+ X\,^1\Sigma^+(v^+=0)$ ion once

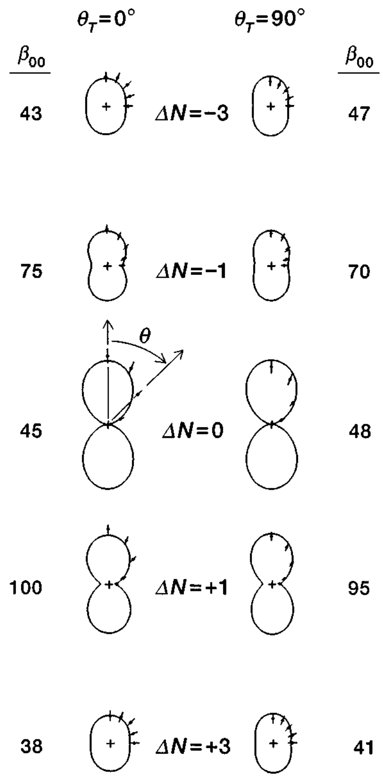

FIG. 3. Polar plots of experimental PADs for five ion rotational levels from photoionization of the NO $D\ ^2\Sigma^+(v=0,\ N=18)$ level. Both the excitation- and the ionization-laser beams are linearly polarized. The plots are scaled to uniform size. The angle-integrated relative cross sections β_{00} are listed with the PADs. Note that the values of β_{00} for $\Delta N>0$ and $\Delta N<0$ transitions with the same $|\Delta N|$ are markedly different. The error bars represent 2σ uncertainties. The solid lines are the predictions of the model based on the fit results listed in the second columns of Tables I through III.

they are uniquely determined from the fit. Whereas $\bar{U}^{\lambda}_{l\alpha_\lambda}$ and $\bar{\tau}^{\lambda}_{\alpha_\lambda}$ represent only the dynamics in the ionization continuum, $M^{\lambda}_{\alpha_\lambda}$ depends both on the ionizing state and on the ionization continuum. Consequently, whereas the same set of $\bar{U}^{\lambda}_{l\alpha_\lambda}$ and $\bar{\tau}^{\lambda}_{\alpha_\lambda}$ are employed to fit quantum-state-specific PADs from the NO A and D states, two distinct sets of $M^{\lambda}_{\alpha_\lambda}$ are employed in the fit depending on the ionizing state: $M^{\lambda}_{\alpha_\lambda}(A)$ designates the electronic dipole-moment matrix element that connects the NO $A\ ^2\Sigma^+(v=0)$ state to the α_λth continuum molecular orbital, and $M^{\lambda}_{\alpha_\lambda}(D)$ denotes the corresponding quantity for the NO $D\ ^2\Sigma^+(v=0)$ state.

Because the ionizing transitions for $\Delta N\geqslant 4$ were not observed in the photoelectron spectra of the NO A and D states,[20,24,26] the partial waves included in our fit were limited to $l\leqslant 3$.[20] This truncation in the partial-wave expansion is also supported by the results of *ab initio* calculations of the corresponding photoionization processes.[36,37] Because of the angular momentum constraint imposed on the one-photon ionizing transition between Σ states, λ is restricted to be either 0 or ± 1. The number of continuum molecular orbitals in the fit is the same as the number of partial-wave channels in the fit, because the molecular orbital and the partial waves are related to each other through a unitary transformation.[27]

According to our formalism, the asymmetry in PADs observed in the photoionization of the NO D state suggests that dynamical parameters that describe the photoionization process are dependent on the photoelectron energy over the energy span of the observed rotational features.[26] In *ab initio* calculations, a Cooper minimum has been proposed to exist in the $3p\sigma\rightarrow d\sigma$ channel at a photoelectron energy around 0.33 eV in the photoionization of the NO $D\ ^2\Sigma^+(v=0)$ state.[37] The Cooper minimum, which is a well-known phenomenon in atomic photoionization,[39,40] refers to a vanishing of the electronic dipole-moment matrix element that connects the ionizing state to one of the ionization channels. Although $\bar{U}^{\lambda}_{l\alpha_\lambda}$, $\bar{\tau}^{\lambda}_{\alpha_\lambda}$, and $M^{\lambda}_{\alpha_\lambda}$ are usually independent of energy over the energy span of several rotational levels,[27] $M^{\lambda}_{\alpha_\lambda}$ associated with the ionization channel that exhibits the Cooper minimum can be strongly dependent on the photoelectron energy because even a small change of the dipole-moment matrix element is important near the point of its vanishing. Therefore, the parameters that signify the linear energy dependences of $M^{\lambda}_{\alpha_\lambda}(D)$ were introduced in the fit for the ionization channels that are related to the $d\sigma$-partial waves in the ionization continuum. Note that one Cooper minimum can cause more than one $M^{\lambda}_{\alpha_\lambda}(D)$ to be dependent on photoelectron energy because several continuum molecular orbitals can have the $d\sigma$-partial-wave component through l mixing in the ionization continuum.[27]

In our previous work,[20,22,24,25] the dynamical parameters in the fit were magnitudes $r_{l\lambda}$ and phases $\eta_{l\lambda}$ of the vibrationally averaged electronic dipole-moment matrix elements that connect an ionizing state to the asymptotic photoelectron partial waves with orbital angular momentum **l** and the projection λ of **l** on the internuclear axis. Unlike $\bar{U}^{\lambda}_{l\alpha_\lambda}$, $\bar{\tau}^{\lambda}_{\alpha_\lambda}$, and $M^{\lambda}_{\alpha_\lambda}$ in the present fit, $r_{l\lambda}$ and $\eta_{l\lambda}$ describe only the dynamics of a specific ionizing state.[20,22,24,25,27] The fitting based on $r_{l\lambda}$ and $\eta_{l\lambda}$ could be decomposed into two independent parts by taking advantage of the photoionization selection rule, $\Delta N+l=odd$, which is applicable for Σ–Σ photoionizing transitions:[41,42] The $\Delta N=$even ionizing transitions were fit with parameters for odd-l partial waves, and $\Delta N=$odd ionizing transitions were fit with parameters for even-l partial waves. This photoionization selection rule does not apply, however, for continuum molecular orbitals that are defined to be the eigenfunction of the short-range electronic Hamiltonian.[27] A continuum molecular orbital can be a combination of even and odd partial waves, depending on the molecular potential that a photoelectron experiences near the molecular-ion core. The electronic transformation matrix elements $\bar{U}^{\lambda}_{l\alpha_\lambda}$ specify the composition of the α_λth continuum molecular orbital in terms of asymptotic partial waves. Therefore, the fit based on $\bar{U}^{\lambda}_{l\alpha_\lambda}$, $\bar{\tau}^{\lambda}_{\alpha_\lambda}$, and $M^{\lambda}_{\alpha_\lambda}$ generally cannot be decomposed into parts unlike the previous fit based on $r_{l\lambda}$ and $\eta_{l\lambda}$.

In principle, the fit based on the formalism presented in PZ1 can determine all the dynamical parameters $\bar{U}^{\lambda}_{l\alpha_\lambda}$, $\bar{\tau}^{\lambda}_{\alpha_\lambda}$, and $M^{\lambda}_{\alpha_\lambda}$, given quantum-state-specific PADs from a sufficient number of electronic states. In the present fit, however, certain parameters on which quantum-state-specific PADs depend weakly cannot be well determined because our experimental data have errors associated with them and also because PADs from only two different electronic states are included in the fit. To determine which dynamical parameters could be obtained from our fit with acceptable confidence, we performed nonlinear least-squares fitting of quantum-state-specific PADs at several stages.

To start with, the fit was performed by ignoring all the short-range interactions that couple the asymptotic partial-wave channels, thus setting the electronic transformation matrix $\mathbf{U}^{\lambda}$ to be a unit matrix. The parameters $\bar{\tau}^{\lambda}_{\alpha_\lambda}$ and $M^{\lambda}_{\alpha_\lambda}$, along with one parameter that signifies the energy dependence of $M^{\lambda}_{\alpha_\lambda}(D)$ for the $d\sigma$-partial wave channel, remained unrestricted throughout the fitting procedure. At the first stage, the fit could be decomposed into two separate parts for even and odd l, as described above for the fit based on $r_{l\lambda}$ and $\eta_{l\lambda}$. At subsequent stages, couplings between partial-wave channels were introduced sequentially by including the appropriate electronic transformation matrix elements as fitting parameters. At each stage, the correlation matrix from the fit was examined carefully to decide whether all the parameters from the fit were determined independently. The goodness of the fit at each stage was judged based on the reduced chi-square value, which is the chi-square value divided by the number of degrees of freedom in the fit. Although the reduced chi-square value in an ideal model fitting should approach 1 statistically,[38] a fit with a reduced chi-square value of less than 2 is considered acceptable in the present case because the experimental PADs contain systematic errors that are not accounted for in our fit. We note that the same criterion was applied in our previous analyses of PADs from the NO $A\ ^2\Sigma^+(v=0, N)$ states that employed $r_{l\lambda}$ and $\eta_{l\lambda}$ as fitting parameters.[20,22,24,25]

At the first stage when the electronic transformation matrix $\mathbf{U}^{\lambda}$ was set to be a unit matrix, the reduced chi-square value from the best converged even-l fit was around 8, which was clearly not acceptable. The reduced chi-square value from the converged odd-l fit was, on the other hand, less than 2 even at this first stage. Investigation of the correlation matrix from the odd-l fit showed no extensive correlations between various parameters in the fit. The result of the odd-l fit suggests, at least statistically, that the short-range interactions that mix even-l and odd-l partial waves are not needed to model the PADs associated with the ΔN=even ionizing transitions. It also implies that each $|l\lambda\rangle$ (l=odd) partial wave forms an independent continuum molecular orbital, that is,

$$\bar{U}^{\lambda}_{l\alpha_\lambda}=\delta_{l\alpha_\lambda} \quad (l=\text{odd},\ \ \lambda=0,1). \tag{1}$$

The result of the even-l fit suggests, on the other hand, that the l-mixing interactions between even-l partial waves are necessary to model the PADs associated with the ΔN=odd ionizing transitions.

Based on observations at the first fitting stage, a fitting parameter that allows the coupling between even-l partial-wave channels was introduced at the second fitting stage. Because only partial waves up to $l=3$ are included in our fit, the even-l block of the electronic transformation matrix becomes a 2×2 matrix for $\lambda=0$. The even-l block for $\lambda=1$ contains, on the other hand, only one element because the partial wave with $l=0$ cannot have a projection $\lambda=1$. Hence, $\bar{U}^{\lambda}_{l\alpha_\lambda}$ for even l can be written as

$$\bar{U}^{\sigma}_{s,sd1}=\bar{U}^{\sigma}_{d,sd2}=\cos(\vartheta^{\sigma}_{sd}), \tag{2a}$$

$$\bar{U}^{\sigma}_{s,sd2}=-\bar{U}^{\sigma}_{d,sd1}=-\sin(\vartheta^{\sigma}_{sd}), \tag{2b}$$

and

$$\bar{U}^{\pi}_{d,\alpha_\lambda}=1. \tag{2c}$$

In Eqs. (2a) through (2c), σ and π represent $\lambda=0$ and $\lambda=1$, respectively. Following the spectroscopic convention, photoelectron partial waves are designated as s, p, d, and f waves for $l=0$, 1, 2, and 3, respectively. The parametrization of $\bar{U}^{\lambda}_{l\alpha_\lambda}$ given in Eqs. (2a) and (2b) ensures that the even-l block of the electronic transformation matrix with $\lambda=0$ is a real unitary matrix. Here, ϑ^{σ}_{sd} represents the mixing angle between the $s\sigma$- and $d\sigma$-partial waves.[16,27] The continuum molecular orbitals formed by the l mixing between the $s\sigma$- and $d\sigma$-partial waves are labeled as $sd1$ and $sd2$ in Eqs. (2a) and (2b). Because $M^{\lambda}_{\alpha_\lambda}(D)$ for both the $sd1$ and $sd2$ ionization channels can be influenced by the Cooper minimum in the $3p\sigma\rightarrow d\sigma$ channel, two fitting parameters that signify the linear energy dependences of $M^{\sigma}_{sd1}(D)$ and $M^{\sigma}_{sd2}(D)$ were included in the fit. Note that only parameter that designates the energy dependence of $M^{\lambda}_{\alpha_\lambda}(D)$ for the $d\sigma$-partial wave channel was included at the first stage of even-l fitting. When the $s\sigma$–$d\sigma$ mixing was introduced in the fit, the reduced chi-square value from the even-l fit dropped below 2. Investigation of the correlation matrix showed no extensive correlations between various parameters at this stage of the even-l fit.

At the third stage, we performed the fitting of quantum-state-specific PADs by introducing fitting parameters that describe mixing between various even-l and odd-l partial waves within the same λ manifold to determine whether the improvement in the reduced chi-square value of the even-l fit resulted from the introduction of two additional fitting parameters. The mixing parameter between the $s\sigma$- and $d\sigma$-partial waves, ϑ^{σ}_{sd}, was, on the other hand, set to be zero, unlike in the second stage, so that the effect of ϑ^{σ}_{sd} could be eliminated in the fit at the third stage. The even-l and the odd-l fit cannot be separated at this stage because the mixing between even-l and odd-l channels is introduced. Up to two parameters were employed in the fit to designate the linear energy dependences of $M^{\lambda}_{\alpha_\lambda}(D)$ for the ionization channels that are coupled to the $d\sigma$-partial-wave channel. Although the fitting was performed exhaustively with new parameters that represent the l mixing between all possible combinations of even-l and odd-l partial waves, the reduced chi-square values were found to be always greater than 4.

Finally, we performed a nonlinear least-squares fitting of PADs with more than one mixing parameter *including* ϑ^{σ}_{sd}.

TABLE I. The continuum parameters determined from the fit of experimental PADs for photoionization of NO via the $A\ ^2\Sigma^+(v=0, N)$ and $D\ ^2\Sigma^+(v=0, N)$ states. Also shown are the values of the corresponding parameters determined from the MQDT analysis of the spectroscopic data of high-lying Rydberg series converging to the $NO^+\ X\ ^1\Sigma^+(v^+=0, N^+)$ ion (Refs. 16 and 43). The values in parentheses represent 1σ uncertainties. Other relative eigenphase shifts (e.g., $\bar{\tau}_f^\pi - \bar{\tau}_f^\sigma$) can be calculated easily from the values listed here.

Parameter	Fit	MQDT analysis
$\bar{\tau}_{sd2}^\sigma - \bar{\tau}_{sd1}^\sigma$	−1.58(3)	−1.25
$\bar{\tau}_d^\pi - \bar{\tau}_{sd1}^\sigma$	−1.28(2)	−1.26
$\bar{\tau}_p^\pi - \bar{\tau}_p^\sigma$	0.070(9)	0.06
$\bar{\tau}_f^\sigma - \bar{\tau}_p^\sigma$	−0.53(9)	−0.65
$\bar{\tau}_f^\pi - \bar{\tau}_p^\sigma$	−0.54(7)	−0.65
ϑ_{sd}^σ	0.73(5)	−0.675

The reduced chi-square values from these fits indeed decreased from the value obtained at the second stage, but only slightly. In addition, the correlations between fitting parameters became more significant as we added more fitting parameters. Combined with the results of the fit at the previous stages, the results of this investigation indicate that in modeling the quantum-state-specific PADs from the NO $A\ ^2\Sigma^+(v=0)$ and $D\ ^2\Sigma^+(v=0)$ states, ϑ_{sd}^σ is statistically more significant than any other single mixing parameter.

The second columns of Tables I through III list all the parameters determined up to the second stage of the fitting procedure described above. These parameters represent the *minimum* set of fitting parameters needed to describe experimental PADs acceptably. As discussed previously, the statistical criterion for the acceptability of the fit was that the reduced chi-square value was less than 2. The dynamical parameters listed in Tables I through III are *signed* quantities except for all $M_{\alpha_\lambda}^\lambda(A)$ and $M_{sd1}^\sigma(D)$ that are constrained to be positive in our fit (see Sec. IV A). The signs of various dynamical parameters could be uniquely determined from our fit with this convention because the quantum-state-specific PADs from the NO $A\ ^2\Sigma^+(v=0, N=22)$ level using the circularly polarized ionization light were included as a data set. The circularly polarized ionization light imposes the handedness to our experimental geometry and enables us to determine the signs of various dynamical parameters.[23,24,30–32]

TABLE II. The vibrationally averaged electronic dipole-moment matrix elements, $M_{\alpha_\lambda}^\lambda(A)$, that connect the NO $A\ ^2\Sigma^+(v=0)$ state to the α_λth continuum molecular orbital. The values in parentheses represent 1σ uncertainties. The second column lists $M_{\alpha_\lambda}^\lambda(A)$ from the unconstrained fit, in which all the parameters were free to vary, and the last column lists $M_{\alpha_\lambda}^\lambda(A)$ from the constrained fit, in which the continuum parameters were fixed at the values obtained from the MQDT analysis of the spectroscopic data of high-lying Rydberg series converging to the $NO^+\ X\ ^1\Sigma^+(v^+=0, N^+)$ ion (see the text). The $M_{\alpha_\lambda}^\lambda(A)$ values are normalized so that their squares sum to unity.

Parameter	Unconstrained fit	Constrained fit
$M_{sd1}^\sigma(A)$	0.271(8)	0.23(1)
$M_{sd2}^\sigma(A)$	0.00(1)	0.13(2)
$M_p^\sigma(A)$	0.50(2)	0.42(2)
$M_f^\sigma(A)$	0.32(2)	0.32(1)
$M_p^\pi(A)$	0.472(9)	0.514(7)
$M_d^\pi(A)$	0.05(1)	0.075(6)
$M_f^\pi(A)$	0.24(1)	0.237(8)

TABLE III. The vibrationally averaged electronic dipole-moment matrix elements, $M_{\alpha_\lambda}^\lambda(D)$, that connect the NO $D\ ^2\Sigma^+(v=0)$ state to the α_λth continuum molecular orbital. The values in parentheses represent 1σ uncertainties. The second column lists $M_{\alpha_\lambda}^\lambda(D)$ from the unconstrained fit, in which all the parameters were free to vary, and the last column lists $M_{\alpha_\lambda}^\lambda(D)$ from the constrained fit, in which the continuum parameters were fixed at the values obtained from the MQDT analysis of the spectroscopic data of high-lying Rydberg series converging to the $NO^+\ X\ ^1\Sigma^+(v^+=0, N^+)$ ion (see the text). The $M_{\alpha_\lambda}^\lambda(D)$ values are normalized so that their squares sum to unity.

Parameter	Unconstrained fit	Constrained fit
$M_{sd1}^\sigma(D)$	0.12(8)	0.02(2)
$M_{sd2}^\sigma(D)$	−0.4(1)	−0.25(2)
$M_p^\sigma(D)$	0.404(7)	0.408(8)
$M_f^\sigma(D)$	0.02(4)	0.02(6)
$M_p^\pi(D)$	0.132(5)	0.132(5)
$M_d^\pi(D)$	0.57(4)	0.607(8)
$M_f^\pi(D)$	−0.01(3)	−0.01(4)
$\frac{1}{M_{sd1}^\sigma(D)} \frac{dM_{sd1}^\sigma(D)}{dE}$ [a]	−0.04(3)	−0.3(2)
$\frac{1}{M_{sd2}^\sigma(D)} \frac{dM_{sd2}^\sigma(D)}{dE}$ [a]	−0.001(2)	−0.008(1)

[a]The energy is in units of the rotational constant of the $NO^+\ X\ ^1\Sigma^+(v^+=0, N^+)$ ion ($B=1.9878\ \mathrm{cm}^{-1}$).

The model PADs predicted for each data set by the dynamical parameters in Tables I through III are shown as solid lines in Figs. 1 through 3. The β_{00} values in Figs. 1 through 3 designate the angle-integrated relative cross sections for each ionizing transition. The experimental PADs in Figs. 1 through 3 from both the NO $A\ ^2\Sigma^+(v=0, N)$ and $D\ ^2\Sigma^+(v=0, N)$ levels agree very well with theoretical predictions based on the simultaneous fit of all the data sets.

III. DISCUSSION

A. Determination of the parameters that describe the ionization continuum

Among the dynamical parameters in our model, the electronic transformation matrix elements $\bar{U}_{l\alpha_\lambda}^\lambda$ and the electronic eigenphase shifts $\bar{\tau}_{\alpha_\lambda}^\lambda$ represent only the dynamics in the ionization continuum and determine various molecule-frame scattering matrices for the photoelectron–ion-core collision up to a phase factor.[27] The second column of Table I lists these continuum parameters determined from the simultaneous fit of quantum-state-specific PADs of the NO $A\ ^2\Sigma^+(v=0)$ and $D\ ^2\Sigma^+(v=0)$ states. In general, the photoionization dynamics and the dynamics in the ionization continuum do not depend on the overall phase of the continuum photoelectron wave function. Consequently, the differences between eigenphase shifts $\bar{\tau}_{\alpha'_{\lambda'}}^{\lambda'} - \bar{\tau}_{\alpha_\lambda}^\lambda$, instead of $\bar{\tau}_{\alpha_\lambda}^\lambda$, are the quantities determined from our fit without arbitrariness, and we list $\bar{\tau}_{\alpha'_{\lambda'}}^{\lambda'} - \bar{\tau}_{\alpha_\lambda}^\lambda$ in Table I. As discussed in Sec. II, the parameters that represent the mixing between even-l and odd-l partial waves were not needed in modeling the experimental PADs, and the fit could be decomposed effectively into two separate parts. Hence the phase relationship between even-l and odd-l partial waves, which can be represented by $\bar{\tau}_{p}^{\sigma} - \bar{\tau}_{sd1}^{\sigma}$, could not be determined from our fit and is omitted from Table I. For the same reason, the electronic transformation matrix for each λ can be decomposed into two independent blocks, one that designates the l-mixing interactions inside the odd-l partial-wave manifold and the other that designates the l-mixing interactions inside the even-l partial-wave manifold. The elements of the former are given in Eq. (1), whereas the elements of the latter can be calculated from Eq. (2) with ϑ_{sd}^{σ} given in Table I.

As described in detail in PZ1, $\bar{\tau}_{\alpha_\lambda}^{\lambda}$ and $\bar{U}_{l\alpha_\lambda}^{\lambda}$ are, respectively, the continuum analogs of the electronic quantum defects and the Rydberg-series mixing coefficients for high-lying Rydberg states. Because $\bar{\tau}_{\alpha_\lambda}^{\lambda}$ and $\bar{U}_{l\alpha_\lambda}^{\lambda}$ characterize the short-range scattering dynamics between the photoelectron and the ion core, they are rather insensitive to the photoelectron energy across the ionization threshold.[27] Considering that photoelectrons observed in our experiments have kinetic energies of only approximately 200 meV, $\bar{\tau}_{\alpha_\lambda}^{\lambda}$ and $\bar{U}_{l\alpha_\lambda}^{\lambda}$ determined from our fit for the continuum photoelectrons can be compared with the electronic quantum defects and the Rydberg-series mixing coefficients, respectively, determined for the high-lying Rydberg states converging to the NO^+ $X\,^1\Sigma^+(v^+=0)$ ion.

The Rydberg series of NO converging to the NO^+ $X\,^1\Sigma^+(v^+=0,\ N^+)$ level have been studied extensively through high-resolution absorption and emission spectroscopy[15,43] and double-resonance MPI spectroscopy.[16] The MQDT analysis of the observed spectra indicates that even-l and odd-l Rydberg series do not interact with each other.[15,16] The analysis also indicates that the interactions among the odd-l Rydberg series are almost negligible whereas the $s\sigma$- and $d\sigma$-Rydberg series almost completely mix to form the so-called "s,d supercomplexes."[15,16] Note that these findings from the MQDT analysis of the Rydberg spectroscopy of NO agree almost completely with the findings from our analysis of quantum-state-specific PADs: The expressions for the electronic transformation matrix given in Eqs. (1) and (2) exactly mirror the findings of the Rydberg spectroscopy.

In the last column of Table I, we list the electronic quantum-defect parameters determined from the spectroscopy of high-lying Rydberg states for quantitative comparison with the dynamical parameters determined in our fit.[16,43] In general, the agreement between the parameters from our fit and the MQDT parameters is satisfactory including signs of $\bar{\tau}_{\alpha'_{\lambda'}}^{\lambda'} - \bar{\tau}_{\alpha_\lambda}^{\lambda}$, despite the small differences between the values of parameters (see below). Two marked discrepancies are apparent in Table I: The sign of ϑ_{sd}^{σ} and the magnitude of $\bar{\tau}_{sd2}^{\sigma} - \bar{\tau}_{sd1}^{\sigma}$.

The sign reversal of ϑ_{sd}^{σ} is believed to originate from the difference in the phase convention employed in this work and in the MQDT analysis of the spectroscopy of high-lying Rydberg states. The $s\sigma - d\sigma$ Rydberg-series mixing coefficient with its sign was determined by Fredin *et al.*[16] through extensive MQDT analysis of the double-resonance MPI spectra of s- and d-Rydberg states via the $C\,^2\Pi$ intermediate state. To determine the sign of the $s\sigma - d\sigma$ Rydberg-series mixing coefficient, Fredin *et al.* calculated the electronic dipole-moment matrix elements for the Rydberg–$C\,^2\Pi$ transitions (which are analogous to $M_{\alpha_\lambda}^{\lambda}$ in our formalism) by employing the assumption that the Coulomb wave functions describe both the $C\,^2\Pi$ state and the Rydberg orbitals. These dipole-moment matrix elements and the signed $s\sigma - d\sigma$ Rydberg-series mixing coefficient were inserted into the MQDT equations to predict the intensity pattern for the Rydberg–$C\,^2\Pi$ transitions. The sign of ϑ_{sd}^{σ} was then determined by comparing the calculated and observed spectra. In these calculations, the signs of dipole-moment matrix elements, which subsequently affect the sign of ϑ_{sd}^{σ} are fixed by the phase convention of Coulomb wave functions.[1]

The actual scattering dynamics between the photoelectron and the ion depends, however, only on the relative phase differences between various ionization channels. Therefore, the signs of dynamical parameters in our fit can be varied simultaneously as long as their variations are correlated so that the dynamically important phase relations between the ionization channels are not changed; inspection of Eq. (34) of PZ1 reveals that the signs of $M_{\alpha_\lambda}^{\lambda}$ are interrelated with the signs of $\bar{U}_{l\alpha_\lambda}^{\lambda}$ and the values of $\bar{\tau}_{\alpha_\lambda}^{\lambda}$ once the phase relations between asymptotic ionization channels are fixed by experimental PADs. As discussed in Sec. II, we determined the signs of all the parameters in the fit by constraining the signs of all $M_{\alpha_\lambda}^{\lambda}(A)$ and $M_{sd1}^{\sigma}(D)$ to be positive. We believe that the difference in the phase conventions in the MQDT analysis of Rydberg spectra and in our fit accounts for the sign reversal of ϑ_{sd}^{σ}. The above discussion also reveals that the close agreement between our fit results and the MQDT parameters in values of $\bar{\tau}_{\alpha'_{\lambda'}}^{\lambda'} - \bar{\tau}_{\alpha_\lambda}^{\lambda}$ is rather fortuitous because they can differ by integer units without affecting the actual scattering dynamics between the photoelectron and the ion when the signs of $M_{\alpha_\lambda}^{\lambda}$ and $\bar{U}_{l\alpha_\lambda}^{\lambda}$ are correlated accordingly. Note that this indeterminacy in $\bar{\tau}_{\alpha'_{\lambda'}}^{\lambda'} - \bar{\tau}_{\alpha_\lambda}^{\lambda}$ is reminiscent of the indeterminacy of quantum defects (and the principal quantum numbers) encountered in the experimental analysis of the Rydberg level positions;[9,16] quantum defects of Rydberg levels can be determined experimentally only up to modulo 1, as is $\bar{\tau}_{\alpha'_{\lambda'}}^{\lambda'} - \bar{\tau}_{\alpha_\lambda}^{\lambda}$ in our analysis. It is nevertheless very clear in Table I that the agreement between the parameters from our fit and the MQDT parameters is very good.

The discrepancies in $\bar{\tau}_{\alpha'_{\lambda'}}^{\lambda'} - \bar{\tau}_{\alpha_\lambda}^{\lambda}$ listed in Table I may reflect real differences between the dynamics of the photoelectron–ion scattering above and below the ionization threshold. It is difficult to explain the marked discrepancy of $\bar{\tau}_{sd2}^{\sigma} - \bar{\tau}_{sd1}^{\sigma}$ based solely on this argument, however, because other $\bar{\tau}_{\alpha'_{\lambda'}}^{\lambda'} - \bar{\tau}_{\alpha_\lambda}^{\lambda}$ show only small discrepancies. The other possible source of this big discrepancy is that $\bar{\tau}_{sd2}^{\sigma} - \bar{\tau}_{sd1}^{\sigma}$ can be determined inaccurately from our nonlinear least-squares fit because of systematic errors present in our data (coupled with the correlations between the various parameters in the fit). The convergence of our fit is achieved by the global minimization of the chi-square value. The fact that we obtained the lowest chi-square value does not guarantee, however, that the various parameters determined from our fit correspond to the true physical parameters in the model, especially because of the systematic errors in the data set.[25,38]

To check this possibility, we performed the nonlinear least-squares fitting of quantum-state-specific PADs with $\bar{\tau}^{\lambda'}_{\alpha'_{\lambda'}} - \bar{\tau}^{\lambda}_{\alpha_\lambda}$ constrained at the values of the corresponding quantum-defect differences obtained from the Rydberg-state spectroscopy. The magnitude of ϑ^{σ}_{sd} was also fixed at the value obtained from the Rydberg-state spectroscopy. The sign of ϑ^{σ}_{sd} was held positive to account for the differences in the phase conventions mentioned previously. Because the interaction between the even-l and odd-l partial-wave manifolds was not detected in the MQDT analysis of the Rydberg spectroscopy, the fit could be decomposed into the odd-l and the even-l parts as before. The fit with the fixed $\bar{\tau}^{\lambda'}_{\alpha'_{\lambda'}} - \bar{\tau}^{\lambda}_{\alpha_\lambda}$ and ϑ^{σ}_{sd} is referred to hereafter as the constrained fit, whereas the fit presented in Sec. II in which $\bar{\tau}^{\lambda'}_{\alpha'_{\lambda'}} - \bar{\tau}^{\lambda}_{\alpha_\lambda}$ and ϑ^{σ}_{sd} are free to vary is referred to as the unconstrained fit. The values of $M^{\lambda}_{\alpha_\lambda}(A)$ and $M^{\lambda}_{\alpha_\lambda}(D)$ [together with two parameters that designate the energy dependences of $M^{\lambda}_{\alpha_\lambda}(D)$] determined from the constrained fit are listed in the last columns of Tables II and III, respectively. The reduced chi-square value from the constrained odd-l fit was less than 2 and was only slightly larger than the reduced chi-square value from the corresponding unconstrained fit. The values of $M^{\lambda}_{\alpha_\lambda}$ ($\alpha_\lambda = l =$odd) were also similar with those determined from the unconstrained fit (see Tables II and III). These results are not surprising considering that $\bar{\tau}^{\lambda'}_{\alpha'_{\lambda'}} - \bar{\tau}^{\lambda}_{\alpha_\lambda}$ ($\alpha_\lambda = l =$odd) determined from the unconstrained fit did not deviate significantly from the corresponding quantum-defect differences. The reduced chi-square value from the constrained even-l fit was, on the other hand, larger than the reduced chi-square value from the unconstrained even-l fit and was close to 2.5.

The model PADs predicted by the dynamical parameters from the constrained fit for the photoionization of the NO $A\,^2\Sigma^+(v=0, N)$ and $D\,^2\Sigma^+(v=0, N=18)$ levels are not presented here because they are virtually indistinguishable from those in Figs. 1 through 3 upon visual inspection. A thorough comparison of model PADs reveals that the increase in the reduced chi-square value of the constrained fit compared with that of the unconstrained fit stems mostly from the failure of the parameters from the constrained fit to account for a few data points in the D-state PADs. As discussed in Ref. 26, the PADs of the NO D state contain more significant systematic errors than the PADs of the NO A state. Therefore, it is quite possible that the failure mentioned above results from systematic errors in the experimental data. This observation implies that the large discrepancy between $\bar{\tau}^{\sigma}_{sd2} - \bar{\tau}^{\sigma}_{sd1}$ determined from the unconstrained fit and the corresponding quantum-defect difference probably originates from the systematic errors present in the experimental PADs of the NO D state. It also implies that with our limited experimental data alone, the small discrepancies between $\bar{\tau}^{\lambda'}_{\alpha'_{\lambda'}} - \bar{\tau}^{\lambda}_{\alpha_\lambda}$ from the unconstrained fit and the corresponding quantum-defect parameters cannot be ascribed to the real difference in the dynamics above and below the ionization threshold.

The above comparison of results from the constrained and unconstrained fits clearly illustrates the difficulty in fitting experimental PADs that contain systematic errors to extract physically meaningful dynamical parameters. The comparison also illustrates, however, that most of the dynamical parameters determined from our analysis of quantum-state-specific PADs are relatively insensitive to the presence of systematic errors in the data. In statistical terms, these parameters determined in our fit can be deemed robust.[38] In addition, although $\bar{\tau}^{\sigma}_{sd2} - \bar{\tau}^{\sigma}_{sd1}$ is found to be sensitive to the presence of systematic errors, only parameters from a small region of the total $U-\tau-M$ parameter space that involves the small variation of $\bar{\tau}^{\sigma}_{sd2} - \bar{\tau}^{\sigma}_{sd1}$ can describe our data acceptably. Therefore, we believe that the parameters determined from our fit are a good representation of true dynamical parameters that describe the ionization continuum of NO associated with NO^+ $X\,^1\Sigma^+(v^+=0)$ and the photoionization of the NO $A\,^2\Sigma^+(v=0, N)$ and $D\,^2\Sigma^+(v=0, N)$ states.

B. Ionization continuum dynamics

The continuum parameters given in Table I and Eqs. (1) and (2) provide a detailed insight into the scattering dynamics between the photoelectron and the NO^+ $X\,^1\Sigma^+(v^+=0)$ ion core. The electronic eigenphase shift $\bar{\tau}^{\lambda}_{\alpha_\lambda}$ is the scattering phase shift for the α_λth continuum molecular orbital, whereas $\bar{U}^{\lambda}_{l\alpha_\lambda}$ is the vibrationally averaged value of the electronic transformation matrix element.[27] Physically, $\bar{\tau}^{\lambda}_{\alpha_\lambda}$ represents the relative attractiveness that the photoelectron in the α_λth continuum molecular orbital experiences *inside* the ion-core region, and $\bar{U}^{\lambda}_{l\alpha_\lambda}$ represents the partial-wave composition of the α_λth continuum molecular orbital. According to the value of $\bar{U}^{\lambda}_{l\alpha_\lambda}$ determined from our fit, the l-mixing interactions between the even-l and odd-l partial waves are not significant. The form of $\bar{U}^{\lambda}_{l\alpha_\lambda}$ for the odd-l partial-wave manifold given in Eq. (1) also indicates that the $|l\lambda\rangle$ ($l=$odd) partial waves do not interact with each other and thus form independent continuum molecular orbitals. Unlike the odd-l partial waves, the $s\sigma$- and $d\sigma$-partial waves are found to be mixed to form continuum molecular orbitals $sd1$ and $sd2$. The magnitude of ϑ^{σ}_{sd} determined from our fit suggests that the mixing between the $s\sigma$- and $d\sigma$-partial waves is almost complete: The composition of the $sd1$ continuum molecular orbital is approximately 55% $s\sigma$ wave and 45% $d\sigma$ wave, whereas the composition of the $sd2$ continuum molecular orbital is 45% $s\sigma$ wave and 55% $d\sigma$ wave. As discussed in Sec. III A, the integral changes in values of $\bar{\tau}^{\lambda'}_{\alpha'_{\lambda'}} - \bar{\tau}^{\lambda}_{\alpha_\lambda}$ are permitted in our fit without changing the actual scattering dynamics between the photoelectron and the molecular ion as long as the correlated changes in signs of $M^{\lambda}_{\alpha_\lambda}$ and $\bar{U}^{\lambda}_{l\alpha_\lambda}$ are accompanied with them. Therefore, the values of $\vec{\tau}^{\lambda'}_{\alpha'_{\lambda'}} - \vec{\tau}^{\lambda}_{\alpha_\lambda}$ listed in Table I cannot be directly interpreted as the relative attractiveness that the photoelectron experiences inside the ion-core region, unless brief physical considerations regarding the penetration[8,44] of the photoelectron into the ion-core region precedes the interpretation.

Semiclassically, photoelectrons with large orbital angular momentum l cannot penetrate into the ion-core region because of the large centrifugal barrier associated with their motion, and the primary characteristic of the ion core that the large-l photoelectron experiences is the charge on the ion. Consequently, partial waves with large l are similar to those in the hydrogenic field. The scattering phase shift (or equivalently the quantum defects) associated with the large-l photoelectron are therefore expected to be small because the scattering phase shift is a measure of the difference between the Coulomb potential and the ion-core potential that photoelectron experiences inside the ion-core region. On the other hand, partial waves with smaller l ($l=0$ and 1) do penetrate into and interact with the ion core. When the photoelectron is deep inside the ion-core region, the effective charge that it experiences can be larger than 1 because of the reduced shielding of the nuclear charge by the other electrons. As a result, the scattering phase shift associated with the small-l photoelectron is expected to be large and negative. Based on these physical considerations, we expect the s- and p-partial waves to be more strongly attracted to the ion core than the d- and f-partial waves, respectively, as observed from the values of $\vec{\tau}^{\lambda'}_{\alpha'_{\lambda'}} - \vec{\tau}^{\lambda}_{\alpha_\lambda}$ listed in Table I. Indeed, the theoretical analysis of Rydberg series of NO essentially confirms these expectations.[14,15] Between orbitals with the same l, the values of $\vec{\tau}^{\lambda'}_{\alpha'_{\lambda'}} - \vec{\tau}^{\lambda}_{\alpha_\lambda}$ listed in Table I indicate that the $p\pi$ wave is found to be more attracted to the core than the $p\sigma$ wave, whereas the $f\sigma$ and $f\pi$ waves are more or less equally attracted to the core.

The fact that mixing between even-l and odd-l partial-wave manifolds is not detected in our fit suggests that the odd-multipolar interactions experienced by the photoelectron in the ion-core region are not strong enough to induce mixing between even-l and odd-l partial waves. The observation that the $s\sigma$- and $d\sigma$-partial waves are completely mixed with each other whereas the p and f waves are relatively unperturbed suggests, on the other hand, that even-multipolar interactions between the photoelectron and the NO^+ $X\,^1\Sigma^+(v^+=0)$ ion inside the ion-core region affect each partial wave differently. As discussed in PZ1, the interaction between the photoelectron and the ion inside the ion-core region is not uniform,[45,46] and the ion-core region can be divided into the multipole-moment-interaction region and the electron-exchange-interaction region.[27] The continuum parameters determined in our fit represent the combined effects of the photoelectron–ion-core interaction in both the multipole-moment-interaction region and the electron-exchange-interaction region. Therefore, to understand the experimental observations in more detail, the interaction between the photoelectron and the NO^+ $X\,^1\Sigma^+(v^+=0)$ ion inside the ion-core region must be examined more closely.

Being a heteronuclear diatomic ion, NO^+ possesses both a dipole moment and a quadrupole moment. The quadrupole moment of the NO^+ $X\,^1\Sigma^+(v^+=0)$ core is particularly significant and is responsible for the λ splitting of the f Rydberg series.[14] The photoelectron-quadrupole interaction in the multipole-moment-interaction region, however, does not seem to be the major cause of $s\sigma$–$d\sigma$ mixing because the experimental PADs did not reveal mixing between p- and f-partial waves which would have been caused by the same interaction. As discussed previously, the interaction between the photoelectron and the dipole in the multipole-moment-interaction region should not be strong enough to cause mixing between the even-l and odd-l partial waves. Therefore, although the interactions between the photoelectron and the multipoles are present in the multipole-moment-interaction region (as evidenced by the λ splitting of the f Rydberg series), they seem not to be significant enough to cause l mixing between different partial waves.

The interaction between the photoelectron and the ion inside the electron-exchange-interaction region can be understood by analyzing the nature of bound molecular orbitals of the NO^+ $X\,^1\Sigma^+(v^+=0)$ ion, as done in the seminal analysis of NO Rydberg-series structures by Jungen.[15] The electronic configuration of the NO^+ $X\,^1\Sigma^+$ ion is given by $1\sigma^2 2\sigma^2 3\sigma^2 4\sigma^2 5\sigma^2 1\pi^4$.[15,37] The single-center expansion of each valence molecular orbital around the center of mass of NO^+ indicates that the 3σ orbital has mostly the $s\sigma$ character, the 4σ orbital has the $p\sigma$ character, and the 1π orbital has the $p\pi$ character. Unlike these molecular orbitals that have single partial-wave characters, the 5σ molecular orbital has both the $s\sigma$ and $d\sigma$ characters. According to Mulliken's terminology,[44] a bound molecular orbital of the ion core is called the precursor of a given Rydberg orbital when the two orbitals have the same λ and approximately the same l values. Considering the close connection between the bound Rydberg orbitals and the partial waves for the continuum photoelectron,[27,44] we can reasonably extend this precursor concept and define the precursor of a given partial wave as the bound molecular orbital that has the same λ and approximately the same l values. Therefore, the 3σ and 5σ orbitals can be considered as precursors for the $s\sigma$-partial wave, and similarly 4σ, 1π, and 5σ orbitals can be considered as precursors for the $p\sigma$-, $p\pi$-, and $d\sigma$-partial waves, respectively.

Within the independent particle approximation, these bound molecular orbitals, or precursors of partial waves, determine the molecular potential with which the photoelectron interacts inside the electron-exchange-interaction region. Because the 5σ orbital is the highest occupied molecular orbital of the NO^+ $X\,^1\Sigma^+$ core with σ symmetry, it contributes more than other orbitals toward determining the molecular potential that the partial waves with σ symmetry experience. Considering that the 5σ orbital is the precursor of both the $s\sigma$- and $d\sigma$-partial waves, the mixing between the $s\sigma$- and $d\sigma$-partial waves appears to be caused mostly by the interaction of the photoelectron with the other electrons inside the electron-exchange-interaction region, especially with the 5σ orbital. On the other hand, the other precursors in the NO^+ $X\,^1\Sigma^+$ core have mostly a single partial-wave character. Therefore, the photoelectron–ion-core interactions inside the electron-exchange-interaction region for partial waves other than $s\sigma$ and $d\sigma$ waves do not result in significant l mixing.

C. Photoionization dynamics of the NO *A* state

The dynamical parameters $\bar{U}^{\lambda}_{l\alpha_\lambda}$, $\bar{\tau}^{\lambda}_{\alpha_\lambda}$, and $M^{\lambda}_{\alpha_\lambda}$ determined from the simultaneous fit of quantum-state-specific PADs from the NO $A\,^2\Sigma^+(v=0)$ and $D\,^2\Sigma^+(v=0)$ states determine not only the dynamics in the ionization continuum but also the photoionization dynamics of the individual ionizing state. Unlike $\bar{U}^{\lambda}_{l\alpha_\lambda}$ and $\bar{\tau}^{\lambda'}_{\alpha'_{\lambda'}} - \bar{\tau}^{\lambda}_{\alpha_\lambda}$ given in Table I, $M^{\lambda}_{\alpha_\lambda}$ depends both on the ionizing state and the ionization continuum because it represents the vibrationally averaged electronic dipole-moment matrix element that connects the ionizing state to the α_λth continuum molecular orbital. Table II lists $M^{\lambda}_{\alpha_\lambda}(A)$ for the photoionization of the NO $A\,^2\Sigma^+(v=0)$ state, and Table III lists $M^{\lambda}_{\alpha_\lambda}(D)$ for the photoionization of the $D\,^2\Sigma^+(v=0)$ state. The photoionization dynamics of the NO $A\,^2\Sigma^+(v=0)$ state has been discussed in detail previously based on the partial-wave decomposition of the ionization continuum.[20,22–25] Because of the disentanglement of the dynamics in the ionization continuum accomplished here based on the molecular-orbital decomposition, however, we can clarify some of the interpretations of the photoionization dynamics of the NO $A\,^2\Sigma^+(v=0)$ state, and emphasis will be given on this clarification in this section.

The NO $A\,^2\Sigma^+$ state is a $3s\sigma$ Rydberg state converging to the NO^+ $X\,^1\Sigma^+$ ion. Therefore, the photoionization selection rule, $l=l_0\pm 1$, for an atomic system for which l_0 is the partial-wave component of the Rydberg electron predicts that the p-partial waves should be dominantly produced in the photoionization process. Our fit results confirm this prediction: according to the value of $M^{\lambda}_{\alpha_\lambda}(A)$ determined in our fit, the p-wave contribution to the total ionization cross section is approximately 70%. The fit results also indicate that the f-wave contribution to the total ionization cross section is more than 20%, whereas the s- and d-wave contributions combined are approximately 10%. Despite this large contribution of the f wave to the total ionization cross section, the $\Delta N=\pm 4$ ionizing transitions are not present in the photoelectron spectrum because of the destructive interference between the dipole-moment matrix elements to the $f\sigma$ and $f\pi$ waves that have comparable magnitudes and phases.[20,22,24,25]

The contribution of $l\neq 1$ partial waves produced in the photoionization of the NO $A\,^2\Sigma^+$ state can be explained either by the l mixing in the ionization continuum or by $l\neq 0$ characters in the NO A state. In *ab initio* calculations, the former has been proposed as the primary cause of the production of partial waves other than p waves.[36,47,48] According to the results of *ab initio* calculations, the p-partial waves generated in the photoexcitation of the $3s\sigma$ orbital are scattered into the $l\neq 1$ partial-wave channels because of the nonspherical molecular potential. As discussed extensively in Sec. IV A, however, the continuum parameters determined in our fit indicate the contrary. According to our fit results, no significant l-mixing interactions occur in the ionization continuum of NO other than the mixing between the $s\sigma$ and $d\sigma$ waves. Because of the limited accuracy of our fit results, we cannot exclude the possibility of small l-mixing interactions between various partial waves. The close agreement between our fit results and the results obtained from the MQDT analysis for the high-lying Rydberg series suggests, however, that the l-changing collisions between the photoelectron and the ion core alone do not account for the production of the $l\neq 1$ partial waves in the ionization continuum.

According to a quantum mechanical calculation using the improved virtual orbital approximation, the single-center expansion of the nominal $3s\sigma$ orbital of the NO $A\,^2\Sigma^+$ state around the center-of-mass yields 94.0% s character, 0.2% p character, 5.5% d character, and 0.1% f character.[48] The calculated magnitudes of the $l\neq 0$ characters in the $3s\sigma$ orbital are not large enough to account for the (s,d)- and f-wave contributions to the total ionization cross section, which are approximately 10% and 20%, respectively. Note, however, that the partial-wave contributions to the ionization cross section are not directly proportional to the partial-wave characters in the ionizing orbital. Instead, they are proportional to the square of the magnitudes of the dipole-moment matrix elements that connect the ionizing orbital to the partial waves in the ionization continuum. The favorable radial overlap between the diffuse $l\neq 0$ components in the $3s\sigma$ orbital and the partial waves in the ionization continuum can result in the large magnitudes of the dipole-moment matrix elements for $l\neq 1$ partial-wave channels, which may explain the observed contributions of $l\neq 1$ partial waves to the total ionization cross section.[49]

D. Photoionization dynamics of the NO *D* state

The rotationally resolved photoelectron spectra[50,51] and the quantum-state-specific PADs[26] from photoionization of the NO $D\,^2\Sigma^+(v=0)$ state have been obtained and analyzed previously to yield the qualitative insight on the photoionization dynamics of the NO $D\,^2\Sigma^+(v=0)$ state. Based on the dynamical parameters determined in our fit, we can obtain a detailed quantitative understanding of the photoionization dynamics of the NO $D\,^2\Sigma^+(v=0)$ state. Indeed, this dynamical information is almost tantamount to determining all the quantum numbers before and after the photoionization process, and it constitutes the complete description of the photoionization of the NO D state.[24] The dynamical parameters obtained in this study also show a clear signature of the existence of the Cooper minimum in the $3p\sigma\rightarrow d\sigma$ ionization channel in the photoionization of the NO D state.[26,37]

The NO $D\,^2\Sigma^+$ state is a $3p\sigma$ Rydberg state converging to the NO^+ $X\,^1\Sigma^+$ ion. The atomic photoionization selection rule predicts the dominant production of s- and d-partial waves in the photoionization of the NO D state, which is indeed confirmed in our fit results. According to $M^{\lambda}_{\alpha_\lambda}(D)$ given in Table III, the combined s- and d-wave contributions account for approximately 80% of the total ionization cross section. The rest of the total ionization cross section is accounted for mostly by the p-wave contribution. The strong asymmetry in intensity between the $\Delta N>0$ and $\Delta N<0$ transitions with the same $|\Delta N|$ is modeled successfully by including two dynamical parameters that signify the *linear* energy dependences of $M^{\sigma}_{sd1}(D)$ and $M^{\sigma}_{sd2}(D)$. The fact that these two parameters can successfully describe the opposite skewing in intensities of the $|\Delta N|=1$ and $|\Delta N|=3$ ionizing transitions is a direct consequence of the interference between various partial waves in the ionization continuum.

As mentioned earlier, the existence of a Cooper minimum in the $3p\sigma\rightarrow d\sigma$ ionization channel was predicted at a photoelectron energy of 0.33 eV in the *ab initio* calculations of Wang, Stephens, and McKoy[37] that are built on the partial-wave decomposition of the ionization continuum. This Cooper minimum occurs because the first radial node of the $d\sigma$-partial wave occurs near the maximum of the outermost loop of the $3p\sigma$ Rydberg orbital. Our fit results indicate that $M^{\sigma}_{sd1}(D)$ and $M^{\sigma}_{sd2}(D)$ are strongly energy dependent at the photoelectron energy of approximately 0.24 eV. Especially, $M^{\sigma}_{sd1}(D)$ goes through zero at this energy, showing a Cooper minimum in the $sd1$ ionization channel. The energy dependences of $M^{\sigma}_{sd1}(D)$ and $M^{\sigma}_{sd2}(D)$ are consistent with the predicted existence of a Cooper minimum in the $3p\sigma\rightarrow d\sigma$ ionization channel because both the $sd1$ and $sd2$ continuum molecular orbitals result from the mixing between the $s\sigma$- and $d\sigma$-partial waves in the ionization continuum. In the experimental quantum-state-specific PADs of the NO D state, the most notable signature for the existence of the Cooper minimum is the strong asymmetry in intensity between the $\Delta N>0$ and $\Delta N<0$ transitions with the same $|\Delta N|$. The appearance of the strong $|\Delta N|=3$ peaks is also illuminating in the context of the occurrence of the Cooper minimum.[26] These peaks result from the d-partial waves in the ionization continuum. As shown in Table I, $\overline{\tau}^{\sigma}_{sd2}$ and $\overline{\tau}^{\pi}_{d}$ are similar in magnitude, indicating that the $sd2$ and $d\pi$ continuum molecular orbitals should interfere destructively. The values listed in Table III indicate that strong $|\Delta N|=3$ peaks are observed despite this destructive interference because of the disparity in the values of $M^{\sigma}_{sd2}(D)$ and $M^{\pi}_{d}(D)$, which is a direct consequence of the Cooper minimum in the $3p\sigma\rightarrow d\sigma$ ionization channel.

The effect of the Cooper minimum in atomic photoionization has been studied extensively since its first identification in photoionization of alkali-metal atoms.[40,52–56] Recently, the importance of the Cooper minimum in molecular Rydberg state photoionization was recognized both theoretically[57–60] and experimentally.[26,61,62] The Cooper minimum in atomic photoionization manifests itself as changes in the total ionization cross sections and the photoelectron angular distributions.[55,56] In molecular photoionization, however, diagnosis of the existence of a Cooper minimum is not so straightforward as in atomic photoionization because of the presence of many ionization channels and the complex interferences between them. The existence of the Cooper minimum in molecular photoionization can be inferred from the strong asymmetry in intensity between the $\Delta N>0$ and $\Delta N<0$ transitions with the same $|\Delta N|$, as observed in the quantum-state-specific PADs of the NO D state in this study and in rotationally resolved photoelectron spectra of Rydberg states of OH[61] and NH.[62] Note, however, that this asymmetry in intensity indicates, the strong energy dependences of dynamical parameters that describe the photoionization process, and thus can be caused by dynamical phenomena other than Cooper minima. The strong appearance of ionizing transitions that involve only partial waves with the same l is also suggestive of a Cooper minimum, as discussed in the preceding paragraph.

It is interesting to note that the same Cooper minimum manifests itself in quite a different manner in the dynamical parameters, depending on whether the dynamical parameters are based on the partial-wave decomposition[24,33,35] or molecular-orbital decomposition of the ionization continuum.[27] Formally, the two descriptions are equivalent in describing photoionization from a given electronic state. In our fit based on the molecular-orbital description of the ionization continuum, $M^{\sigma}_{sd1}(D)$ is found to change sign and show a strong energy dependence consistent with the original definition of the Cooper minimum as a vanishing of the dipole-moment matrix element for one of the ionization channels. Because of the l mixing, however, $r_{l\lambda}$ and $\eta_{l\lambda}$, which are based on the partial-wave description of the ionization continuum, show more complex energy dependences when the Cooper minimum exists for one of the ionization channels.[59] As discussed earlier, $s\sigma$- and $d\sigma$-partial waves are formed by the interference between the $sd1$ and $sd2$ continuum molecular orbitals. Hence, the energy dependences of $M^{\sigma}_{sd1}(D)$ and $M^{\sigma}_{sd2}(D)$ in our fit translate into the complex variations of not only the magnitudes, $r_{s\sigma}$ and $r_{d\sigma}$, but also the phases, $\eta_{s\sigma}$ and $\eta_{d\sigma}$, of the partial-wave dipole-moment matrix elements. Indeed, in *ab initio* calculations, the Cooper minimum in the $3p\sigma\rightarrow d\sigma$ ionization channel shows up as the sign change of the standing-wave-normalized principal part of the dipole-moment matrix element for the $d\sigma$ ionization channel, whereas the magnitude of the dipole-moment matrix element itself does not undergo the sign change.[37] A more detailed comparison of our fit results and the results of *ab initio* calculations is impossible at the moment because $\eta_{s\sigma}$ and $\eta_{d\sigma}$ are not reported in Ref. 37.

The single-center expansion of the nominal $3p\sigma$ orbital of the NO $D\,^2\Sigma^+$ state around the center-of-mass yields 0.62% s character, 98.77% p character, 0.56% d character, and 0.07% f character, according to a quantum-mechanical calculation using the improved virtual orbital approximation.[37] On the other hand, the results of our fit indicate that the p-wave contribution to the total ionization cross section amounts to almost 20%. This seemingly large discrepancy between the small s and d characters in the $3p\sigma$ orbital and the large p-wave contribution in the ionization continuum may result, at least partly, from the presence of the Cooper minimum mentioned above.[37] Because of the smallness of the dipole-moment matrix elements for the $d\sigma$ ionization channel caused by the Cooper minimum, the relative importance of the p-wave contribution becomes larger at the photoelectron energy observed in our experiment.

Another possible explanation for the large p-wave contribution is that the s and d characters in the NO D state may be enhanced by interaction with the other electronic state. Absorption and emission studies have shown that the NO $D\,^2\Sigma^+(\nu=0)$ state is heterogeneously perturbed by vibrational levels of the $B\,^2\Pi$ state.[63,64] Although the NO $D\,^2\Sigma^+(\nu=0,\ N=18)$ level employed in this study is not directly perturbed by this heterogeneous interaction,[34] the perturbation is conceivably enough to enhance the s and d characters in the NO D state. We also note that even a perturbation between the NO $A\,^2\Sigma^+(\nu=4)$ and $D\,^2\Sigma^+(\nu=0)$ states, which would certainly enhance the s character in the NO D state, has been proposed although definite spectroscopic evidence is currently lacking.[51]

Within the context of the formalism presented in PZ1, the dynamical parameters listed in Tables I through III provide all the information necessary to predict total system states after photoionization of the NO $A\,^2\Sigma^+(\nu=0)$ and $D\,^2\Sigma^+(\nu=0)$ states.[24] From the dynamical parameters, we can predict unambiguously the rotational state distribution of the ion, including its alignment and orientation, the three-dimensional PADs, and all possible correlations between various vector quantities.[24,65] Indeed, combined with information on the total ionization cross sections for photoionization of the NO $A\,^2\Sigma^+(\nu=0)$ and $D\,^2\Sigma^+(\nu=0)$ states,[66,67] the dynamical parameters given in Tables I through III provide a complete description of the photoionization of the NO $A\,^2\Sigma^+(\nu=0)$ and $D\,^2\Sigma^+(\nu=0)$ states.[23–25,28,29] A complete description of the photoionization of the NO D state is achieved without the measurement of CDAD from the NO D state because we have analyzed the experimental PADs from the NO A and D states simultaneously using the formalism presented in PZ1. As noted at the end of Sec. II, the CDAD data set from the NO A state alone enables us to determine the signs of all the dynamical parameters, even those for the NO D state. This determination, which would have been impossible within the formalism based on the partial-wave decomposition of the ionization continuum,[22,23,25] clearly illustrates the advantage of the present formalism, which exploits to the fullest extent possible the commonality between two distinct photoionization processes.

IV. CONCLUSION

We have presented an analysis of quantum-state-specific PADs from the NO $A\,^2\Sigma^+(\nu=0)$ and $D\,^2\Sigma^+(\nu=0)$ states based on the theoretical formalism developed in PZ1. The parameters obtained in this analysis determine not only the photoionization dynamics of the NO A and D states but also the dynamics of the ionization continuum associated with the NO^+ $X\,^1\Sigma^+(\nu^+=0)$ ion. Through this study, we have shown that analysis of the quantum-state-specific PADs can yield detailed information on the short-range scattering dynamics between the photoelectron and the NO^+ $X\,^1\Sigma^+(\nu^+=0)$ ion, which agrees very well with the quantum-defect parameters determined from the spectroscopic analysis of high-lying Rydberg series. This information is tantamount to determining the molecule-frame scattering matrices that describe the collision events between the photoelectron and the ion and represents the first such determination in the molecular system. The dynamical parameters obtained in this study also constitute complete descriptions for photoionization of the NO A and D states, and thus enable us to predict various unobserved dynamical quantities associated with the NO^+ $X\,^1\Sigma^+(\nu^+=0)+e^-$ system accessed by the individual photoionization process. They also provide a detailed quantitative insight into the existence of a Cooper minimum in the $3p\sigma\rightarrow d\sigma$ ionization channel for the photoionization of the NO $D\,^2\Sigma^+(\nu=0)$ state.

ACKNOWLEDGMENTS

H.P. is grateful for a Franklin Veatch Memorial Fellowship from Stanford University. We acknowledge the support of the National Science Foundation under Grant No. PHY-9320356.

[1] M. J. Seaton, Rep. Prog. Phys. **46**, 167 (1983).
[2] K. T. Lu, Phys. Rev. A **4**, 579 (1971).
[3] C.-M. Lee and K. T. Lu, Phys. Rev. A **8**, 1241 (1973).
[4] J. C. Hansen, J. J. A. Duncanson, R.-L. Chien, and R. S. Berry, Phys. Rev. A **21**, 222 (1980).
[5] U. Heinzmann, J. Phys. B **13**, 4367 (1980).
[6] M. D. Lindsay, C.-J. Dai, L.-T. Cai, T. F. Gellagher, F. Robicheaux, and C. H. Greene, Phys. Rev. A **46**, 3789 (1992).
[7] Y.-Y. Yin and D. S. Elliott, Phys. Rev. A **47**, 2881 (1993).
[8] R. S. Mulliken, Acct. Chem. Res. **9**, 7 (1976).
[9] C. H. Greene and Ch. Jungen, Adv. At. Mol. Phys. **21**, 51 (1985).
[10] D. Dill and J. L. Dehmer, J. Chem. Phys. **61**, 692 (1974).
[11] R. R. Lucchese and V. McKoy, Phys. Rev. A **24**, 770 (1981).
[12] P. C. Burke, in *Collision Theory for Atoms and Molecules*, edited by F. A. Gianturco (Plenum, New York, 1989), p. 11.
[13] U. Fano, Phys. Rev. A **2**, 353 (1970).
[14] Ch. Jungen and E. Miescher, Can. J. Phys. **47**, 1769 (1969).
[15] Ch. Jungen, J. Chem. Phys. **53**, 4168 (1970).
[16] S. Fredin, D. Gauyacq, M. Horani, Ch. Jungen, G. Lefevre, and F. Masnou-Seeuws, Mol. Phys. **60**, 825 (1987).
[17] W. G. Wilson, K. S. Viswanathan, E. Sekreta, and J. P. Reilly, J. Phys. Chem. **88**, 672 (1984).
[18] K. Müller-Dethlefs, M. Sander, and E. W. Schlag, Chem. Phys. Lett. **112**, 291 (1984).
[19] S. T. Pratt, P. M. Dehmer, and J. L. Dehmer, J. Chem. Phys. **85**, 3379 (1986).
[20] S. W. Allendorf, D. J. Leahy, D. C. Jacobs, and R. N. Zare, J. Chem. Phys. **91**, 2216 (1989).
[21] E. de Beer, M. Born, C. A. de Lange, and N. P. C. Westwood, Chem. Phys. Lett. **186**, 40 (1991).
[22] D. J. Leahy, K. L. Reid, and R. N. Zare, J. Chem. Phys. **95**, 1757 (1991).
[23] K. L. Reid, D. J. Leahy, and R. N. Zare, Phys. Rev. Lett. **68**, 3527 (1992).
[24] D. J. Leahy, K. L. Reid, H. Park, and R. N. Zare, J. Chem. Phys. **97**, 4948 (1992).
[25] H. Park and R. N. Zare, J. Chem. Phys. **99**, 6537 (1993).
[26] H. Park and R. N. Zare, Chem. Phys. Lett. **225**, 327 (1994).
[27] H. Park and R. N. Zare, J. Chem. Phys. **104**, 4554 (1996).
[28] B. Bederson, Comments At. Mol. Phys. **1**, 41 (1969).
[29] J. Kessler, Comments At. Mol. Phys. **10**, 47 (1981).
[30] R. L. Dubs, S. N. Dixit, and V. McKoy, Phys. Rev. Lett. **54**, 1249 (1985).
[31] R. L. Dubs, S. N. Dixit, and V. McKoy, J. Chem. Phys. **85**, 656 (1986).
[32] J. R. Appling, M. G. White, R. L. Dubs, S. N. Dixit, and V. McKoy, J. Chem. Phys. **87**, 6927 (1987).
[33] S. N. Dixit and V. McKoy, J. Chem. Phys. **82**, 3546 (1985).
[34] C. Amiot and J. Verges, Chem. Phys. Lett. **66**, 570 (1979).
[35] K. L. Reid, D. J. Leahy, and R. N. Zare, J. Chem. Phys. **95**, 1746 (1991).
[36] H. Rudolph and V. McKoy, J. Chem. Phys. **91**, 2235 (1989).
[37] K. Wang, J. A. Stephens, and V. McKoy, J. Chem. Phys. **95**, 6456 (1991).

[38] W. H. Press, B. P. Flannery, S. A. Teukolsky, and W. T. Vetterling, *Numerical Recipes* (Cambridge University, Cambridge, 1986).
[39] U. Fano and J. W. Cooper, Rev. Mod. Phys. **40**, 441 (1968).
[40] S. T. Manson, Phys. Rev. A **31**, 3698 (1985).
[41] S. N. Dixit and V. McKoy, Chem. Phys. Lett. **128**, 49 (1986).
[42] J. Xie and R. N. Zare, J. Chem. Phys. **93**, 3033 (1990).
[43] E. Miescher and K. P. Huber, in *International Review of Science* (Butterworths, London, 1976), Vol. 2, p. 37.
[44] R. S. Mulliken, J. Am. Chem. Soc. **86**, 3183 (1964).
[45] E. S. Chang and U. Fano, Phys. Rev. A **6**, 173 (1972).
[46] Ch. Jungen and O. Atabek, J. Chem. Phys. **66**, 5584 (1977).
[47] S. N. Dixit, D. L. Lynch, V. McKoy, and W. M. Huo, Phys. Rev. A **32**, 1267 (1985).
[48] H. Rudolph, S. N. Dixit, V. McKoy, and W. M. Huo, J. Chem. Phys. **88**, 637 (1988).
[49] W. Y. Cheung, W. A. Chupka, S. D. Colson, D. Gauyacq, P. Avouris, and J. J. Wynne, J. Chem. Phys. **78**, 3625 (1983).
[50] K. S. Viswanathan, E. Secreta, E. R. Davidson, and J. P. Reilly, J. Phys. Chem. **90**, 5078 (1986).
[51] X. Song, E. Sekreta, J. P. Reilly, H. Rudolph, and V. McKoy, J. Chem. Phys. **91**, 6062 (1989).
[52] R. W. Dichtburn, J. Tunstead, and J. G. Yates, Proc. R. Soc. London, Ser. A **181**, 386 (1943).
[53] D. R. Bates, Proc. R. Soc. London, Ser. A **188**, 350 (1947).
[54] J. W. Cooper, Phys. Rev. **128**, 681 (1962).
[55] Y.-Y. Yin and D. S. Elliott, Phys. Rev. A **45**, 281 (1992).
[56] Y.-Y. Yin and D. S. Elliott, Phys. Rev. A **46**, 1339 (1992).
[57] W. A. Chupka, J. Chem. Phys. **87**, 1488 (1987).
[58] J. A. Stephens and V. McKoy, Phys. Rev. Lett. **62**, 889 (1989).
[59] J. A. Stephens and V. McKoy, J. Chem. Phys. **93**, 7863 (1990).
[60] K. Wang, J. A. Stephens, and V. McKoy, J. Phys. Chem. **97**, 9874 (1993).
[61] E. de Beer, C. A. de Lange, J. A. Stephens, K. Wang, and V. McKoy, J. Chem. Phys. **95**, 714 (1991).
[62] K. Wang, J. A. Stephens, V. McKoy, E. de Beer, C. A. de Lange, and N. P. C. Westwood, J. Chem. Phys. **97**, 211 (1992).
[63] Ch. Jungen and E. Miescher, Can. J. Phys. **46**, 987 (1968).
[64] C. Amiot and J. Verges, Phys. Scr. **25**, 302 (1982).
[65] H. Park, Ph.D. thesis, Stanford University, 1995. For example, it can be shown that the alignment of the $\mathbf{N}^+$ vectors of the NO^+ $X\ ^1\Sigma^+(v^+=0)$ ion generated by the $\Delta N=0$ photoionizing transition of the NO $D\ ^2\Sigma^+(v=0)$ state is quite different from that of the $\mathbf{N}$ vectors in the latter, which suggests the occurrence of pure alignment transfer in elastic scattering between the photoelectron and the NO^+ ion core.
[66] H. Zacharias, R. Schmiedl, and K. H. Welge, Appl. Phys. **21**, 127 (1980).
[67] H. Rottke and H. Zacharias, J. Chem. Phys. **83**, 4831 (1985).